

Multi-Axis Maglev Nanopositioner for Precision Manufacturing and Manipulation Applications

Shobhit Verma

Student Member, IEEE

Dept. of Mechanical Engineering
Texas A&M University
College Station, TX, 77843-3123
shobhit@tamu.edu

Won-jong Kim

Senior Member, IEEE

Dept. of Mechanical Engineering
Texas A&M University
College Station, TX, 77843-3123
wjkim@mengr.tamu.edu

Huzefa Shakir

Student Member, IEEE

Dept. of Mechanical Engineering
Texas A&M University
College Station, TX, 77843-3123
huzefa@tamu.edu

Abstract—We present a 6-axis magnetic levitation (maglev) stage capable of precision positioning down to several nanometers. This stage has a simple and compact mechanical structure advantageous to meet the performance requirements in the next-generation nanomanufacturing. It uses the minimum number of linear actuators required to generate all 6-axis motions. Three vertical actuators are used to levitate the moving part, namely the platen, and maintain its vertical position. Other three horizontal actuators control its position and rotation in the horizontal plane. In this paper, we describe the electromechanical design, modeling and control, and the electronic instrumentation to control this maglev system. We modeled the platen as a pure mass due to negligible spring and damping forces while it is levitated without contact. The stage has a light moving-part mass of 0.2126 kg. It is capable of generating translation of 300 μm in the x -, y - and z -axes, and rotation of 3 mrad about the three orthogonal axes. The stage demonstrates position resolution better than 5 nm rms and position noise less than 2 nm rms. The total power consumption by all the actuators is only a fraction of a watt. Experimental results presented in this paper show that the stage can carry, orient, and precisely position a payload as heavy as 0.3 kg. The pull-out force was found to be 8.08 N in the vertical direction. Furthermore, under the effect of a load variation of 0.14 N, the plant recovers its regulated position within 0.6 s. All these experimental results match quite closely with the calculated values because of the accurate plant model and robust controller design. This device can be used as a positioning stage for numerous applications including photolithography for semiconductor manufacturing, microscopic scanning of delicate instruments, fabrication and assembly of nano-structures, and microscale rapid prototyping.

Keywords—precision motion control; magnetic levitation; permanent-magnet machine; system modeling and control; Lorentz-force linear actuator.

I. INTRODUCTION

Positioning stages have been used in the industry for various applications in machining, coordinate measuring, scanning for profile sensing, etc. The need of precision-positioning stages increased drastically due to their crucial role in the fabrication of micro- and nano-sized objects and assemblies. The key role of a nanopositioning stage is to load, position, and orient such an object and keep it stable without much vibration or noise. Most significant requirements for the

actuators in nanomanipulation include accuracy, range of motion, degrees of freedom, and bandwidth [1]. Commonly used devices for micromanipulation are scanning tunneling microscopes (STMs) and atomic force microscopes (AFMs). Most of these manipulation devices are actuated by piezoelectric materials [2]–[3]. However, there are certain challenges with the piezoelectric actuation systems. (1) The accuracy is greatly influenced by thermal drift under temperature variation. (2) The hysteresis in piezoelectric materials reduces the repeatability in positioning. (3) A slow creeping motion after a large voltage step results in a significant positioning error [4]. The motion capability of these devices is usually limited to linear motions with a short travel range of around 100 μm .

For a long period of time researchers have been looking for solutions to single-axis or multi-axis nanopositioning. Egshira *et al.* developed a high-speed precision stage with a resolution of 0.69 nm using a non-resonant-type ultrasonic motor [5]. A high-bandwidth linear actuator capable of generating 1-nm steps without overshoot or undershoots was fabricated by Mori *et al.* [6]. Sun *et al.* demonstrated a dual-axis electrostatic microactuation system, which is capable of 0.01- μm resolution in 5- μm position change [7]. A high-stiffness linear piezoelectric motor with a resolution of 5 nm and output force of 200 N was presented by Zhang and Zhu [8].

The magnetic levitation technology has been successful for nanopositioning applications. Several research groups have developed precision positioning devices using this technology. The main benefit of magnetic levitation over other technologies is its non-contact nature while in operation, i.e. the forces are applied to the moving part without any mechanical contact. Since the moving part is levitated in the air, there is no friction, hysteresis, or backlash. Kim *et al.* constructed a 6-DOF (degree-of-freedom) high-precision planar maglev stage with large planar motion capability that had 10-nm position resolution and 100-Hz control bandwidth [9]–[10]. Holmes *et al.* fabricated a maglev scanning stage with three-sigma horizontal position noise of 0.6 nm [11]. Jung and Baek designed and demonstrated a 6-DOF maglev positioner with self-stability for 5 DOFs [12].

Among the various potential applications of this maglev nanopositioning device is the manufacture of small objects. This stage in conjunction with other manufacturing technologies that can provide with fabrication and assembly at micro-level will be able to produce micro-sized objects. In such applications this maglev stage will be used as the positioning device and the fabrication/scanning of parts can be done with a fixed tool. One of such techniques is micro-stereolithography (μ STL). Classical STL processes use a laser beam deflected by a pair of low-inertia-galvanometric mirrors and focused by a dynamic lens to solidify the polymer. This methodology works well for objects on the order of a few hundred micrometers. However, beam defocusing becomes problematic for smaller objects. An alternate approach is to keep the laser beam fixed and use a high-precision positioning stage for generating x - y motion for scanning [13]. Beluze *et al.*, Zhang *et al.* and Jiang *et al.* have used this kind of x - y stages for μ STL [14–16]. Ikuta *et al.* showed the capability of such stages for the mass integrated harden polymer stereolithography process [17]. However, in all these processes, the minimum achievable part size is limited by the position resolution of the stage being used. In this paper, we have demonstrated that this limitation in positioning can be easily overcome with our maglev stage.

In Section II, we present the mechanical design and assembly of the maglev stage, linear permanent-magnet unit actuators, and sensors and instrumentation system. Section III covers the plant modeling and control system design. This is followed by numerous experimental results in Section IV to demonstrate the performance of the stage under various payloads, abrupt load variations, and experimental verification of the pull-out force. In Section V, we show the precision motion capabilities of the maglev stage with the test results of generating a variety of single- and multiple-axis motion profiles. Finally, the need and utility of this research is summarized in Section VI with an emphasis on industrial applications.

II. THE 6-DEGREE-OF-FREEDOM MAGLEV STAGE

A. Mechanical Design and Assembly

We developed a compact single-moving-part maglev stage. A photograph of the assembly is shown in Fig. 1. The moving-part assembly consists of a single-piece triangular aluminum platen pocket-milled to reduce the mass while maintaining the structural stiffness. There are three layers on the top of the platen, an aluminum top plate, a viscoelastic damping layer, and a stainless-steel constraint layer. The assembly of these three layers adds passive damping to the system to minimize the structural vibrations and improve the stability. There is no iron part in the assembly, which eliminates the eddy current and helps making the system controllable at high bandwidth. The mass of this platen assembly is just 0.2126 kg, and the total power consumption by all the actuators is only a fraction of a watt. There are 3 sets of arms protruded on the sides of the platen to hold 6 cylindrical magnets for horizontal actuation. The other 3 magnets are attached on the bottom surface for vertical actuation. The coils for all six actuators are mounted on an aluminum base plate via coil holders. There are 3 plane mirrors attached to the sides of the platen for horizontal motion

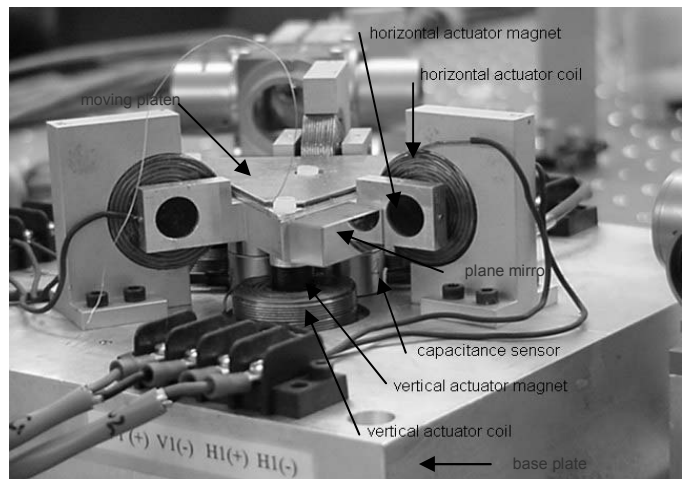


Fig. 1. Photograph of the nanopositioning maglev stage

sensing. Vertical motion sensing is accomplished by 3 capacitance sensors mounted on the base plate right below the platen.

B. Linear Permanent-Magnet Unit Actuators

The 6-axis motion generation by the platen is achieved by the application of 6 independent force components. The directions of the forces generated by the actuators are shown in Fig. 2. Each unit actuator consists of one coil epoxied to its coil-holder and one or two magnets with their spacer or mount. The vertical actuators have one magnet, and the horizontal actuators have two magnets. There is a small spacer that has been glued between the magnets in the horizontal actuator. The thickness of this spacer 4 mm was estimated by a force calculation equation for maximum-force generation. We used cylindrical neodymium-iron-boron (NdFeB) magnets with the energy product (BH_{max}) of 0.4 MJ/m³ (50 MGOe) with diameter of 11.684 mm and the height of 9.525 mm. The coils were wound with heavy-built AWG#21 copper magnet wire that had a layer of heat-bondable epoxy coating on it. Each coil has 179 turns with the resistance of 0.552 Ω and the inductance of 0.5 mH. The average nominal current in each vertical actuator is 0.7 A, so the nominal I^2R power consumption in each actuator is 0.27 W and the whole actuator system is 0.81 W to support the platen weight against the gravity. The coils

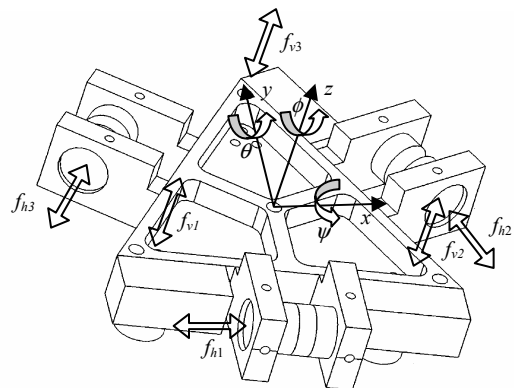


Fig. 2. Convention of the coordinate axes and the directions of forces generated by the unit linear actuators

have the inner diameter of 12.2 mm, the outer diameter of 32.5 mm on average, and the height of 9.55 mm. The current-carrying coil generates the N or S pole based on the direction of the current governed by the right-hand rule. Depending on its magnetization direction, an attractive or repulsive force is applied on the magnet. The reversal of the direction of the current will change the direction of the applied force. The precise assembly of the coils and magnets was a crucial task as the magnet-coil gap is just 0.504 mm, and a small error in assembly would lead to the reduction in the travel range. Thus we designed and fabricated fixtures for precision assembly of the coils with their holders and the magnets with their spacers. The complete characterization of these actuators was described by Kim and Maheshwari [18].

C. Sensors and Instrumentation System

We use a VME (Versa Module Eurocard) chassis as a communication backbone among various electronics boards. This VME chassis has a VME PC (VMIC 7751), a DSP (digital signal processor) board (Pentek 4284), a 16-bit data-acquisition board (Pentek 6102), and 3 laser-axis boards (Agilent 10897B). The DSP board has a TMS320C40 DSP by Texas Instruments. It takes care of all the foreground computing tasks in real-time control. It gathers the position and velocity data from the laser-axis boards and the data-acquisition board, takes user commands or predefined positions and trajectories, applies the control law, calculates the control outputs, and generates the output commands via DACs (digital-to-analog converters) also available on Pentek 6102. All the above tasks are accomplished in an interrupt service routine (ISR) initiated by hardware interrupt at every 200 μ s.

The actual position and velocity measurements of the platen are essential for real-time control. The 3-axis position and velocity in the horizontal plane (x -, y -translation, and ϕ -rotation) is sensed by laser interferometers. The three plane mirrors mounted on the platen reflect the He-Ne laser beam, and the receiver gives the raw data to the laser-axis boards for processing. The laser-axis boards output at 10 MHz 35-bit position and 24-bit velocity data that are received by the DSP via the VMEbus.

We use 3 capacitance gauges (ADE 2810) for vertical position sensing. These gauges face the bottom surface of the platen to sense its height at 3 different locations. With a triangulation method we calculate the z -translation and ψ - and θ -rotations. The outputs of these gauges are fed to their signal conditioning boards (ADE 3800). The ADE 3800 boards give the analog signals corresponding to the platen position in the vertical axes. We sample the analog signals and convert them to digital data using ADCs (analog-to-digital converters) on Pentek 6102. These sensor data are used by the real-time digital controller. To avoid the aliasing of the sensor signals by higher frequency noise contents we use a set of first-order RC anti-aliasing filters with a cut-off frequency at approximately 1 kHz right before sampling by the ADCs.

The control outputs indicating desired coil currents are given to 6 transconductance amplifiers. These amplifiers are connected to the coils to flow the commanded currents. The output swing of the DACs is ± 5 V and the current limit in the

coils is set ± 2.5 A. The output current from an amplifier is linearly proportional to the input voltage. Each amplifier consists of a differential amplifier to reject the common-mode noise, a feedback amplifier to stabilize the current-control loop, and a power booster with a power operational amplifier (PA12A) by Apex.

III. SYSTEM MODELING AND CONTROL

In this section we present the modeling of the maglev stage. Then a decoupled control strategy is discussed.

A. Plant Modeling

We built a 3D model of the whole maglev system with Solidworks and carried out finite-element analyses to identify various system parameters. The lowest natural frequency of the platen was found to be 4.6 kHz. Since the platen is magnetically levitated in the absence of any contact, the spring and damping effects are negligible. Thus we model the platen as a pure mass, and the equation of motion for translation is

$$M \frac{d^2x}{dt^2} = f, \quad (1)$$

where M is the mass of the platen, i.e. 0.2126 kg and f is the corresponding modal force. Thus the transfer function of the platen for translation is

$$\frac{X(s)}{F(s)} = \frac{1}{0.2126 s^2}. \quad (2)$$

Similarly the transfer function of the platen for rotation is

$$\frac{\Theta(s)}{T(s)} = \frac{1}{I s^2}, \quad (3)$$

where I is the moment of inertia about the corresponding axis. The values of principal moments of inertia, I_{xx} , I_{yy} , and I_{zz} are 133×10^{-6} , 122×10^{-6} , 236×10^{-6} kg-m², respectively.

B. Control System Design

A decoupled lead-lag controller was designed on the basis of the dynamic model derived in the previous section. The damping ratio (ζ) was 0.7, and the phase margin was 50° at a crossover frequency of 48 Hz. To eliminate the steady-state error a free pole was placed at the origin in the s -plane.

$$G(s) = K \frac{(s+130)(s+8)}{s(s+1130)}, \quad (4)$$

where K is the gain of the controller, which is 6.7897×10^4 N/m for x -, y -, and z -translation. For rotation, the values of K are 42.438 N, 39.052 N, and 75.329 N for ψ , θ , and ϕ , respectively. We used the zero-order-hold (ZOH) equivalence method to convert this continuous-time controller to a discrete-time one with a 5-kHz sampling frequency and implemented it on the DSP as a difference equation.

IV. LOAD TESTS

In this section, we present various load-test results to demonstrate the maglev stage's dynamic performance for nanomanufacturing and μ STL applications. In these applications, the positioner is supposed to carry small, but time-varying loads.

A. Payload vs. Current

Experiments were carried out with various payloads applied to the platen in the form of dead-weights. The currents in the vertical actuators to maintain the platen position constant were measured. A plot of payload vs. applied current is shown in Fig. 3. The small circles shown in the figure are the experimental data points for various loads and the line connecting them is the least-square linear fit by MATLAB. This linear relation between the coil current and the force is as expected because the generated force is directly proportional to the coil current in our Lorentz-force unit linear actuator. From the experimental data we found the force constant to be 0.798 N/A after subtracting the force offset of 2.09 N to balance the weight of the platen. We also numerically calculated the theoretical Lorentz force, $\mathbf{f} = \int (\mathbf{J} \times \mathbf{B}) dV$ using Mathcad, with which the force constant was found to be 0.839 N/A. Thus the error between the experimental force constant and its theoretical value is only 5%. A possible cause of the error may be inaccurate reading of data due to small continuous fluctuation in current while in closed loop, and manufacturing and assembly errors.

B. Pull-Out Force

We performed an experiment to determine the pull-out force of the maglev stage. We attached a spring at the center of the platen and applied a vertical force on it. The spring was pulled upwards manually, so the amount of the force was continuously increasing. Fig. 4 shows the platen position in z and the control effort f_z applied by the controller to maintain the platen position constant. The z -axis position of the platen shifted suddenly at around 0.425 s indicating the pull-out force of 7.75 N. The actuators are designed to deliver maximum current of 2.5 A with the force constant of 0.798 N/A. Thus the maximum force that the controller can apply via the three vertical actuators to maintain the platen position would be $3 \times 0.798 \text{ N/A} \times 2.5 \text{ A} = 5.99 \text{ N}$. Since the direction of the pull-out force is upwards, it balances the platen weight and then overcomes the vertical actuator forces. The force to balance the weight of the platen would be $0.2126 \text{ kg} \times 9.81 \text{ m/s}^2 = 2.09 \text{ N}$. Thus the theoretical value of the pull-out force will be $5.99 \text{ N} + 2.09 \text{ N} = 8.08 \text{ N}$. The error in the experimental value is only about 4%.

C. Step Responses with Various Payloads

To test the dynamic performance of the maglev stage, several step responses were taken with various payloads. The experimental results are shown in Fig. 5. The stage was able to levitate and position an additional mass of 0.3 kg on the platen. The payloads of more than 0.4 kg made the stage unstable due to actuator saturation in the overshoot. The additional payload increases the mass, keeping the system stiffness about the

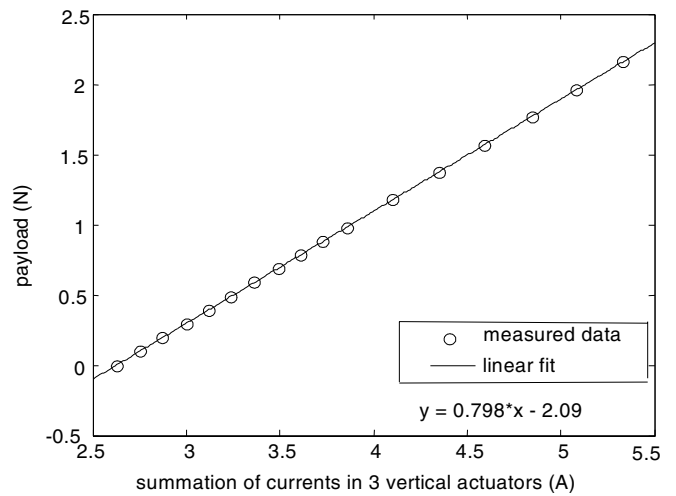


Fig. 3. Payload vs. current required to maintain the platen position constant

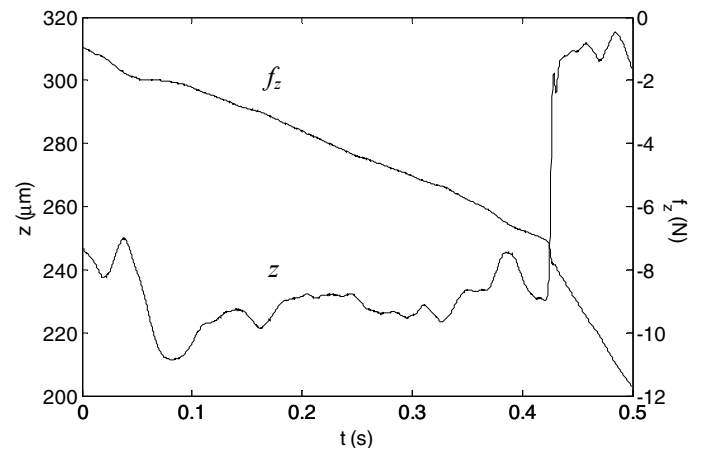


Fig. 4. Determination of the pull-out force with the vertical position z of the platen and the control effort f_z to maintain the platen position constant

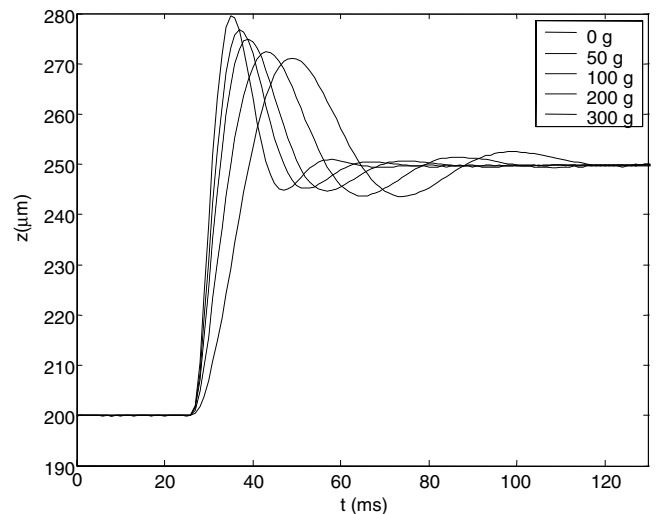


Fig. 5. No-load and load tests with 50- μ m step responses in z with 0-g, 50-g, 100-g, 200-g, and 300-g added masses

same, which lowers the natural frequency of the moving platen. Due to the lower natural frequency the rise time and the settling time are longer for the larger payloads as shown in the figure.

D. Recovery from Sudden Load Changes

To test the response of the platen for sudden load changes we placed small ceramic cylinders on the platen. We recorded the z -axis position and the control effort f_z by the controller to recover the position of the platen still under 6-axis magnetic levitation when the two ceramic cylinders were taken off. Fig. 6(a) shows the plot of the z -axis position, and Fig. 6(b) shows the control effort. The load removal occurred at 0.78 s and 2.35 s, which generated perturbations in z . In the beginning of this experiment the vertical actuators were applying the forces precisely sufficient to balance the weight of the platen and the payload. As soon as the payload was removed, the applied force became greater than that to balance the weight of the platen and the payload. This excessive force gave the platen an instantaneous push upwards that was recovered by the controller over a period of 0.6 s. The maglev system's behavior was repeatable for the second load removal. It can be observed from Fig. 6(b) that the control effort in z decreased as soon as a ceramic cylinder was removed. The drop in the control effort was measured to be 0.14 N for first ceramic cylinder and 0.135 N for the second cylinder. The mass of each cylinder was 14 g i.e. 0.137 N. This shows that the error between the experimental control effort and the actual force is only around 2%.

E. Recovery from Continuously Varying Load

We used a continuous flow of sand falling into a bowl placed on the platen to emulate the effect of the continuously varying load in nanomanufacturing and μ STL applications. The

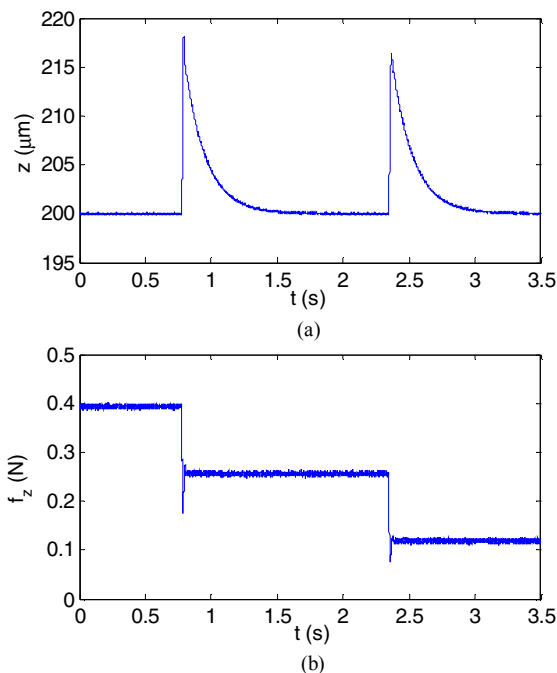


Fig. 6. (a) Position in z and (b) control effort f_z by the controller under sudden load changes. Each 14-g ceramic cylinder was removed at $t = 0.78$ and 2.35 s.

z position of the platen is shown in Fig. 7(a) and corresponding control effort required is shown in Fig. 7(b). From the initial steady-state position, the mass inflow was initiated at 3 s and was stopped at 11 s; then started again at 16 s and stopped at 22 s. Since the rate of the mass change was almost constant, the control effort linearly increased to balance the additional mass on the platen and to regulate the vertical position of the platen at the same level. However, there was a small steady-state error in the vertical position during the mass variation, which acts like a force disturbance at the control input. This is attributed to the fact that the plant poles are not identically located at zero, and the controller was originally designed to meet the zero-steady-state error requirement for the position inputs with a single pole at the origin.

V. PRECISION MOTION CONTROL

In addition to its load capacity demonstrated in the previous section, we present in this section the maglev stage's nanoscale multi-axis motion generation capability.

A. Nanoscale Periodic Motions

The maglev stage is capable of generating precise trajectories. In Fig. 8(a) a sinusoidal waveform of a 50-nm amplitude is shown, and the platen followed the commanded path very well. There were no large overshoots, and the noise level was consistently less than 3 nm rms while in motion. Fig. 8(b) shows a square-wave motion of the platen between two positions with the distance of 40 nm. The dashed lines represent shows the commanded path, and the solid lines represent the resultant path traversed by the platen. While taking steps from one point to the other, there was an overshoot of around 15 nm. It settled down almost instantaneously and brought back the noise level to the minimum. This

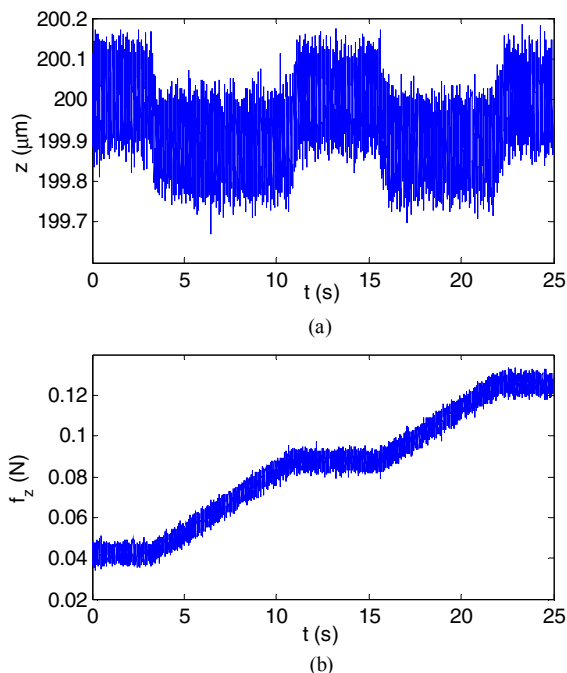


Fig. 7. (a) Position in z and (b) control effort f_z by the controller under continuously varying load

demonstrates that the maglev system can track commanded trajectories very precisely and fast, which is advantageous for precision positioning applications that need agile motions.

B. Nanoscale Consecutive Steps

Fig. 9 shows the platen responses to 15-nm consecutive step commands at every 0.5-s time interval. The position repeatability is better than 2 nm. Fig. 9(b) and (c) show the errors in x and y while generating these steps. The tracking error in x has peaks at every 0.5 s due to the abrupt changes in position. The regular noise level in x is close to 3 nm rms mainly due to these perturbations. The error in the y -axis is maintained below 2 nm rms. This shows that there is very little dynamic coupling between the x - and y -axes. In other words, no sudden change in x affects the y -axis motion, and the controller (4) is robust enough to keep the platen stable.

C. 100-nm Ramp Responses

In Fig. 10 the commanded path for the platen is an up-and-down ramp with the peak of 100 nm. Fig. 10(a) shows the actual path traversed by the platen. It is visible from the figure that the starting point of the trajectory is not exactly zero. This is due to nanoscale position noise in the stage. The peaks of the

trajectory appear to be at around 105 nm and -5 nm instead of 100 nm and 0 nm because of the overshoots at the ends of the ramp trajectories. The path is more distorted near the ends due to the abrupt change in the direction of motion.

D. 2D Circular Motion

In the real-time control code written in the C language as an ISR, a set of data points in more than one axis can be allocated with respect to time so that the platen can follow a multi-axis trajectory. In Fig. 11(a), a commanded path of a 50-nm-radius circle and the response of the platen are shown. The trajectory errors in x and y in this nanoscale circular motion are shown in Fig. 11(b) and (c). We demonstrated that this stage could follow nanoscale 2-dimensional paths precisely.

E. 3D Motion Generation for Micromanufacturing

We performed several experiments to test the performance of the maglev stage with complex 3D commanded paths. Among them a bowl-shaped trajectory with a parabolic vertical cross-section is shown in Fig. 12. The platen closely followed the trajectory. The commanded point changed to make the platen move in a circular path by adding 1° rotation about the center at every sampling period of 200 μ s.

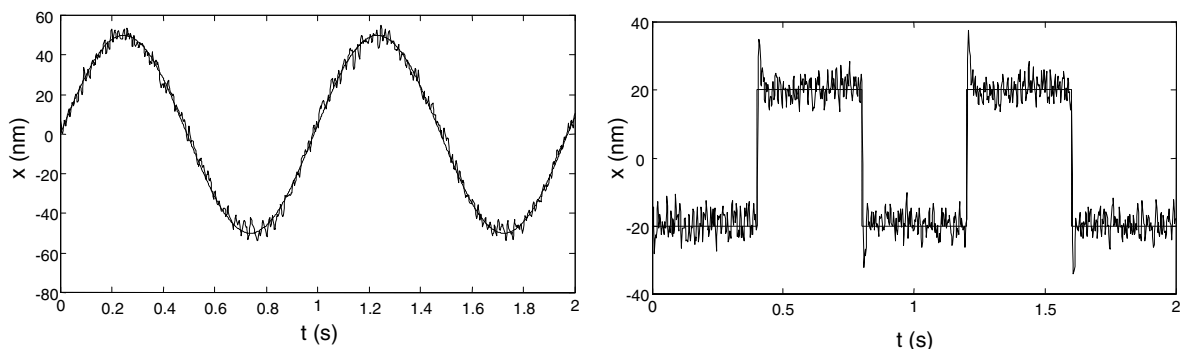


Fig. 8. (a) 50-nm-amplitude sinusoidal motion in x . (b) 20-nm-amplitude square-wave motion in x . The dashed lines represent the commanded, and the solid lines represent the actual trajectories traversed by the platen.

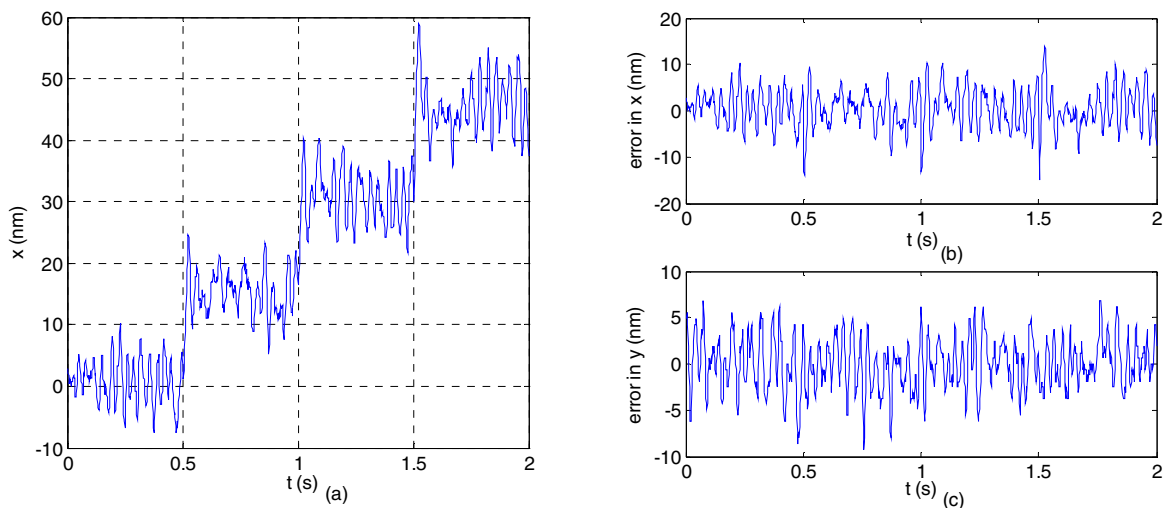


Fig. 9. (a) 15-nm consecutive step at 0.5 s; (b) error in x and (c) error in y while generating these steps

Fig. 13 shows a 3D trajectory followed by the platen layer by layer in the way as desired for μ STL to prove this maglev stage's positioning capability in micromanufacturing. The generated shape is of an impeller that has an outer radius of 25 μm and inner radius of 10 μm . The maglev stage was made to follow this whole 3D motion trajectory in only 18 s, although the platen would need to be moved much slower in an actual μ STL process to allow sufficient time for the photopolymer to cure. These experimental results demonstrate the microscale 3D motion-generation capability of the maglev stage.

VI. CONCLUSIONS

Nanomanipulation has become an essential tool for the development of current nanotechnology. Nanopositioning stages that have higher resolution in multiple axes with large travel ranges are in demand. In this paper, we presented the electromechanical design and control of such a maglev stage as a promising solution for nanopositioning applications. This maglev stage has a simple mechanical structure without significant nonlinearity, which reduces the manufacturing cost and improves the dynamic performance. Its modeling and control system design were discussed in the paper. The dynamic performance of the system was demonstrated with

various experiments.

Step responses with various payloads showed that the derived plant model was accurate. The calculated parameters of the unit actuators such as their force-constants were found to be sufficiently accurate, and experiments clearly showed that the force vs. current behavior of the actuators was linear in the operating range as expected. The pull-out force was 7.75 N from experiments which matched closely with the calculated value of 8.08 N. Furthermore sudden changes in load did not make the system unstable, and the controller could recover a load variation of 0.14 N within 0.6 s and brought back the platen to the commanded position.

In practical applications, the presence of external forces in the form of payload variation or mass fluctuation is inevitable. For instance, in μ STL, the mass of the substrate may vary as the photopolymer is solidified. Similarly, in micro-scanning applications, the load may vary in cantilever-probe-type scanning. Furthermore, there may be abrupt changes in external forces on the stage during contact mode operations. Apparently, in all these applications, the anticipated load variation is much less than the load capacity of the maglev stage demonstrated in section IV. Thus this stage guarantees a smooth vibration-free performance for the applications

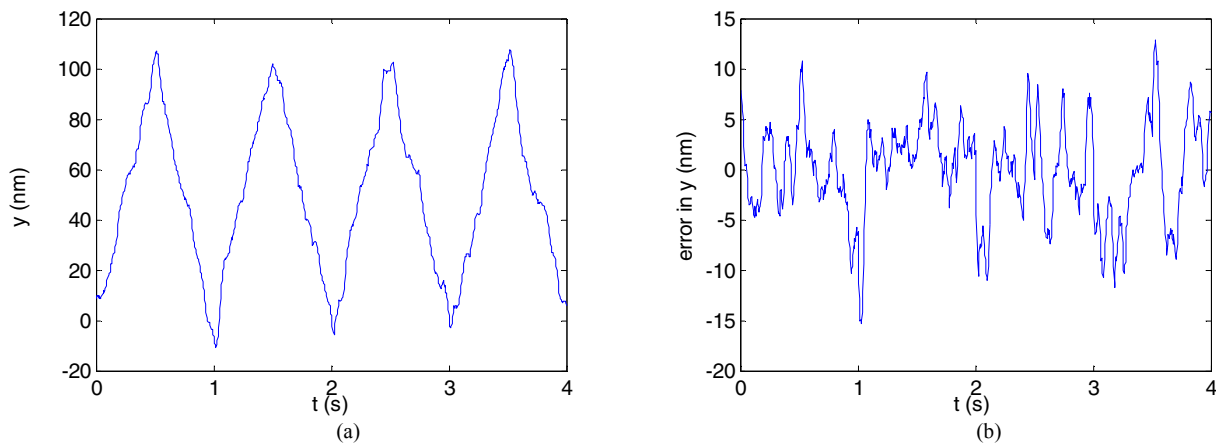


Fig. 10. (a) 100-nm up-and-down ramp response in y and (b) tracking error while the platen was following the commanded path

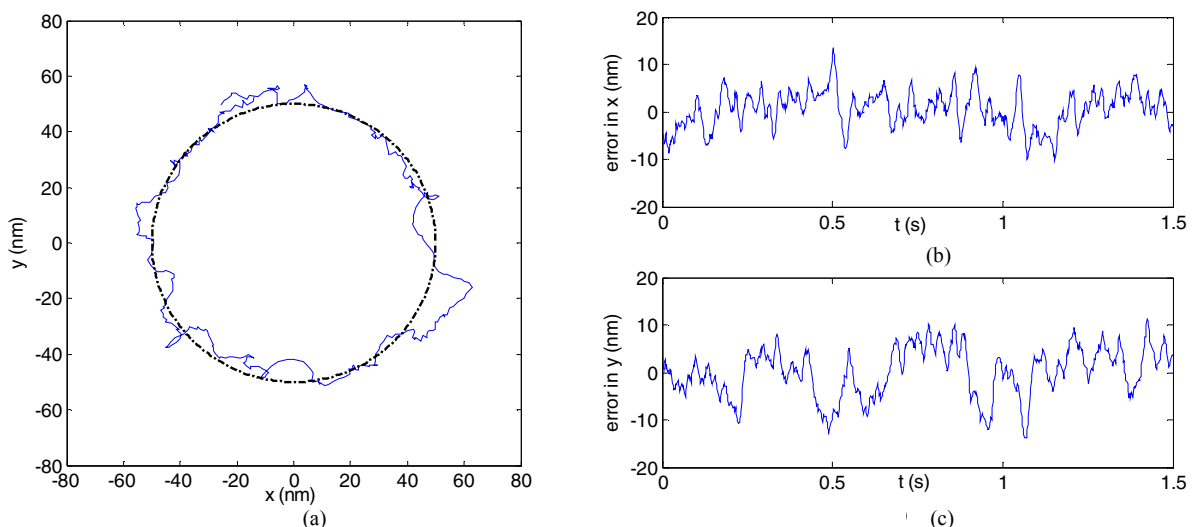


Fig. 11. (a) 50-nm-radius circle traversed in the x - y plane with commanded path and followed path; (b) error in x and (c) error in y

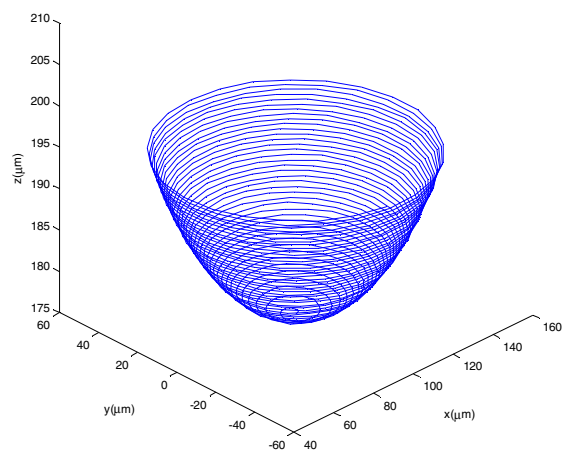


Fig. 12. A bowl with parabolic shape with a 20- μm height and 100- μm maximum radius traversed by platen

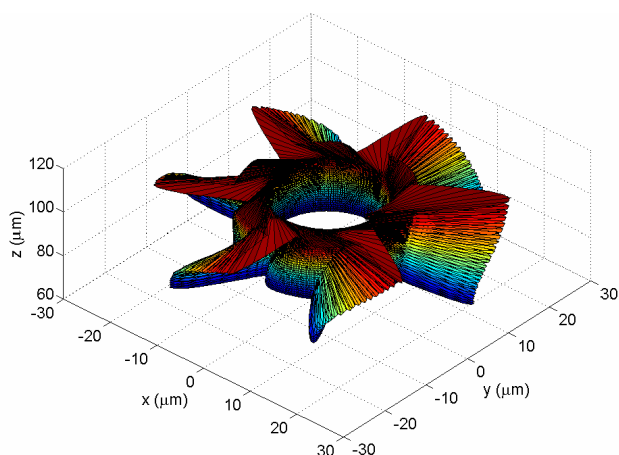


Fig. 13. A 3D impeller shape traversed by the platen

requiring precision positioning/scanning even in the presence of load fluctuations.

The platen was tested to track several 1D, 2D, and 3D trajectories. These experimental results proved that this device was very successful in following complex paths with only nanometer-order tracking errors. This maglev stage that can generate complex multi-axis motions has numerous applications including ultra-fine machining, precision positioning for scanning and characterization, manufacture of nanoscale structures, atomic-level manipulation, vibration isolation for delicate instruments, seismic motion detection, and micro-scale rapid prototyping.

ACKNOWLEDGMENTS

This material is based on the work supported by the National Science Foundation under the Grant No. CMS-0116642. Authors thank Jie Gu for his contribution in design and software development.

REFERENCES

- [1] M. Sitti, "Survey of nanomanipulation systems," *Proc. IEEE-NANO 2001*, pp. 75–80, October 2001.
- [2] R. M. Taylor, *The Nanomanipulator: A Virtual-Reality Interface to a Scanning Tunneling Microscope*, Ph.D. Dissertation, University of North Carolina at Chapel Hill, Chapel Hill, NC, 1994.
- [3] M. F. Yu, M. J. Dyer, H. W. Rohrs, X. K. Lu, K. D. Ausman, J. V. Her, and R. S. Ruoff, "Three-dimensional manipulation of carbon nanotubes under a scanning electron microscope," *Nanotechnology*, vol. 10, no. 3, pp. 244–252, September 1999.
- [4] A. A. G. Requicha, S. Meltzer, A. F. P. Terán, J. H. Makaliwe, H. Sikén, S. Hsieh, D. Lewis, B. E. Koel, and M. E. Thompson, "Manipulation of nanoscale components with the AFM: Principles and applications," *Proc. IEEE-NANO 2001*, pp. 81–86, October 2001.
- [5] Y. Egshira, K. Kosaka, S. Takada, T. Iwabuchi, T. Baba, S. Moriyama, T. Harada, K. Nagamoto, A. Nakada, H. Kubota, and T. Ohmi, "0.69 nm resolution ultrasonic motor for large stroke precision stage," *Proc. IEEE-NANO 2001*, pp. 397–402, October 2001.

- [6] S. Mori, T. Hoshino, G. Obinata, and K. Ouchi, "Linear actuator with air bearing for highly precise tracking [HDD]," *Digest of the Asia-Pacific Magnetic Recording Conference*, pp. AP4-01–AP4-02, May 2002.
- [7] Y. Sun, D. Piyabongkam, A. Sezen, B. J. Nelson, R. Rajamani, R. Schoch, and D. P. Potasek, "A novel dual-axis electrostatic microactuation system for macromanipulation," *Proc. of IEEE/RSJ Intl. Conf. on Intelligent Robots and Systems*, pp. 1796–1801, October 2002.
- [8] B. Zhang and Z. Zhu, "Developing a linear piezomotor with nanometer resolution and high stiffness," *IEEE/ASME Tr. on Mechatronics*, vol. 2, no. 1, pp. 22–29, March 1997.
- [9] W.-J. Kim, *High-Precision Planar Magnetic Levitation*, Ph.D. Dissertation, Massachusetts Institute of Technology, Cambridge, MA, June 1997.
- [10] W.-J. Kim and D. L. Trumper, "High-precision magnetic levitation stage for photolithography," *Precision Engineering*, vol. 22, no. 2, pp. 66–77, April 1998.
- [11] M. Holmes, R. Hocken, and D. L. Trumper, "The long-range scanning stage: a novel platform for scanned-probe microscopy," *Precision Engineering*, vol. 24, no. 3, pp. 191–209, July 2000.
- [12] K. S. Jung and Y. S. Baek, "Study on a novel contact-free planar system using direct drive DC coils and permanent magnets," *IEEE/ASME Tr. on Mechatronics*, vol. 2, no. 1, pp. 35–43, March 2002.
- [13] V. K. Vardan, X. Jiang and V. V. Vardan, *Microstereolithography and other Fabrication Techniques for 3D MEMS*, John Wiley and Sons Ltd., 2001, pp. 111–127.
- [14] L. Beluze, A. Bertsch and P. Renaud, "Microstereolithography: A new process to build complex 3D objects," *Proc. SPIE*, vol. 3680, pp. 808–817, April 1999.
- [15] X. Zhang, X. N. Jiang and C. Sun, "Microstereolithography of polymeric and ceramic microstructures," *Sensors and Actuators A (Physical)*, vol. A77, no. 2, pp. 149–156, March 1999.
- [16] X. N. Jiang, C. Sun, X. Zhang, B. Xu, and Y. H. Ye, "Microstereolithography of lead zirconate titanate thick film on silicon substrate," *Sensors and Actuators A (Physical)*, vol. A87, no. 1-2, pp. 72–77, May 2000.
- [17] K. Ikuta, S. Maruo, and S. Kojima, "New microstereolithography for freely movable 3D microstructure—super IH process with submicron resolution," *Proc. IEEE MEMS*, pp. 290–295, January 1998.
- [18] W.-J. Kim and H. Maheshwari, "High-precision control of a maglev linear actuator with nano-positioning capability," *Proc. of 2002 American Control Conference*, pp. 4279–4284, May 2002.